AIAA 2003–0952

Efficient Development of High Fidelity Structured Volume Grids for Hypersonic Flow Simulations

Stephen J. Alter
NASA Langley Research Center
Hampton, Virginia 23681-2199

41st AIAA Aerospace Sciences Meeting and Exhibit
January 6–9, 2003/Reno, NV

Efficient Development of High Fidelity Structured Volume Grids for Hypersonic Flow Simulations

Stephen J. Alter*
NASA Langley Research Center Hampton, Virginia 23681-2199

A new technique for the control of grid line spacing and intersection angles of a structured volume grid, using elliptic partial differential equations (PDEs) is presented. Existing structured grid generation algorithms make use of source term hybridization to provide control of grid lines, imposing orthogonality implicitly at the boundary and explicitly on the interior of the domain. A bridging function between the two types of grid line control is typically used to blend the different orthogonality formulations. It is shown that utilizing such a bridging function with source term hybridization can result in the excessive use of computational resources and diminishes robustness. A new approach, Anisotropic Lagrange Based Trans-Finite Interpolation (ALBTFI), is offered as a replacement to source term hybridization. The ALBTFI technique captures the essence of the desired grid controls while improving the convergence rate of the elliptic PDEs when compared with source term hybridization. Grid generation on a blunt cone and a Shuttle Orbiter is used to demonstrate and assess the ALBTFI technique, which is shown to be as much as 50% faster, more robust, and produces higher quality grids than source term hybridization.

Nomenclature

α_{ij}	Second derivative coefficients in the elliptic system of PDEs
β_l	Decay rate coefficient for source term blending
ΔS	Distance between two points
ϵ	Stretching factor between two adjacent cells
γ_{ij}	Cofactors of the coordinate transformation from the computational to the physical domain
$\Phi_{u,v,w}$	TFI blending function for the ξ-,η-, and ζ-directions
$\Psi_{u,v,w}$	Bi-linear TFI blending function with exponential decay in the ξ-,η-, and ζ-directions
$\Omega_{u,v,w}$	Bi-quadratic TFI blending function with exponential decay in the ξ-,η-, and ζ-directions
$\theta\|_{\zeta=constant}$	Grid line intersection angle at a constant ζ-plane
Θ	Grid line straightness measure
J	Jacobian of the transformation
i,ξ	Streamwise computational direction and index measured from nose to tail of body ranging from 1 to a maximum number of points
j,η	Circumferential computational direction and index from top to bottom of body ranging from 1 to a maximum number of points
k,ζ	Computational direction and index normal to body surface ranging from 1 to a maximum number of points
p_l	Incremental source term at face l
P	Source term controlling the cell sizes and angles ξ-direction
Q	Source term controlling the cell sizes and angles η-direction
R	Source term controlling the cell sizes and angles ζ-direction
$\vec{r}$	Position vector of x, y, and z
u, v, w	Univariate interpolation functions corresponding to the $\xi-, \eta-$, and ζ-directions
X, Y, Z	Cartesian coordinates

Introduction

There are several methods available to generate structured grids, from algebraic to partial differential equations (PDEs). The solution of an elliptic set of PDEs provides the most control over the grid line character that can promote the development of high fidelity grids, in both spacing and grid line intersections. The most common elliptic PDE in use for structured grid generation is Poisson's equation. This equation provides both smooth distributions of grid points which occur at simulated isothermal line intersections from the homogeneous portion (i.e., the Laplace equation), with control of the grid line character provided by the

*Senior Aerospace Engineer, Senior Member AIAA

particular solution from the source terms.

Assumptions about grid line incidence and cell height at a boundary are used to develop source terms[1-4] for the PDEs. Source terms that control these characteristics have been formulated for specific conditions. Hence, the effect they have on the grid can vary significantly. For example, the specifications for cell size and incidence angle posed by Steger and Sorenson[1] (S&S) are usually decayed into the interior of the domain, so that the Poisson equation will satisfy an extrema principal which is needed to prevent the overlapping of grid lines. The grid line incidence controls of Thomas and Middlecoff[4] (T&M) make some gross assumptions about the grid to obtain nearly orthogonal intersections on the interior. The dilemma is that neither produces enough control on the boundary and interior towards development of a high fidelity grid; characterized by minimal grid stretching and significant orthogonality at intersecting grid lines. Source terms available were unable to produce high fidelity grids because the S&S source terms have very little effect on the interior, while the T&M source terms have no guarantee of imposing an orthogonal character of the grid at a boundary. Early successes of the generation of high fidelity grids were achieved through the introduction of source term hybridization which combines the effects of S&S at a boundary with the effects of T&M on the interior. Source term hybridization is accomplished by decaying implicit source terms such as the S&S onto the interior, while exponentially adding explicit source terms such as the T&M. The intention was to provide the best attributes of both formulations of source terms. However, the coupling makes no accommodation for the undesired characteristics of both source term formulations such as conflicts for the directions for grid point movement between both source term formulations. This deficiency is usually the root of many problems with source term hybridization. For example, the implicit source terms may impose a non-orthogonal character to the grid lines at a boundary, in contrast to the explicit source terms which are formulated by assuming orthogonality, which results in inconsistent state of source terms. The conflict in these conditions of the grid controls are then reflected by the inability of a grid generation solver to obtain converged solutions of the elliptic PDEs. Therefore, a more efficient mechanism is needed to couple the implicit characteristics of S&S with grid line intersection controls on the interior.

This paper presents a new alternative to source term hybridization for the generation of high fidelity structured volume grids. The new approach, called Anisotropic Lagrange Based Trans-Finite Interpolation (ALBTFI) utilizes a multiple variable blending function to amalgamate the implicit source terms of S&S and H&W at all six faces of a computational domain onto the interior. The ALBTFI scheme, already posed in two dimensions,[3] is extended to three dimensions and modified through the incorporation of exponential decay functions, while incorporating both S&S and H&W source terms, which improve robustness of volumetric grid generation. Additionally, a different form of the PDEs, than White, is used. To verify the benefits of ALBTFI versus source term hybridization simple sphere cone and Space Shuttle Orbiter geometries are used to illustrate the improved efficiency, robustness and quality of the new approach.

Grid Control for High Fidelity

To consider the effect that a new modification has on the development of high fidelity structured grids, several issues need to be addressed. These include:

[1] Mechanisms to control grid line character;

[2] quantification of quality; and

[3] grid resolution as it affects the efficiency of performing CFD simulations.

Issues 1 and 2 are addressed below, while issue three is deferred to work to be presented in another paper. Though not exclusive, these attributes provide a basis for the construction of high fidelity structured volume grids. Mechanisms to control grid line character in an elliptic smoother can be decomposed into two different types of source terms; implicit and explicit. Implicit source terms apply a set of boundary conditions and update the source terms in the elliptic PDE until those conditions are achieved. Explicit source terms assume a specific boundary condition, which results in a set of source terms that are held constant throughout the convergence of the elliptic PDEs to a steady state solution. Measuring the quality of a grid enables the determination of the applicability of the chosen boundary conditions to obtain the desired grid fidelity.

Assessing Grid Quality

Grid quality is usually assessed using a variety of measures, as they relate to the problem being solved. Typically the extent of orthogonality, identified by

$$\theta|_{\xi=constant} = \frac{2}{\pi}\cos^{-1}\left(\frac{\vec{r}_\eta \cdot \vec{r}_\zeta}{|\vec{r}_\eta||\vec{r}_\zeta|}\right) \quad (1a)$$

$$\theta|_{\eta=constant} = \frac{2}{\pi}\cos^{-1}\left(\frac{\vec{r}_\xi \cdot \vec{r}_\zeta}{|\vec{r}_\xi||\vec{r}_\zeta|}\right) \quad (1b)$$

$$\theta|_{\zeta=constant} = \frac{2}{\pi}\cos^{-1}\left(\frac{\vec{r}_\xi \cdot \vec{r}_\eta}{|\vec{r}_\xi||\vec{r}_\eta|}\right) \quad (1c)$$

and a typical stretching is determined using the equation 2, which serves as a template for the other computational directions.

$$\epsilon_\xi = \frac{max\left(|\vec{r}_\xi|^+, |\vec{r}_\xi|^-\right)}{min\left(|\vec{r}_\xi|^+, |\vec{r}_\xi|^-\right)} \quad (2a)$$

The orthogonality measure ranges from unity to purely orthogonal grid line intersections to zero which represent collapsed cells, and the stretching measure ranges from unity for uniform spacing to infinity for highly stretched grids. More specific restraints are placed on grid grid quality when considering hypersonic flow regimes. For hypersonic flow fields, where grid adaptation is essential for the placement of grid densities to resolve boundary layer properties, and removal of grid points from the freestream region while preserving the outer bow shock location, grid line straightness in the body to shock direction improves the efficacy of grid adaptation. The body to shock direction is typically used for grid adaptation because this direction is most efficient at resolving both boundary layer properties as well as shock wave location. Curved grid lines in this direction tend to cause wave like patterns to be developed in the grid along the remaining computational directions of the flow domain. The wave like patterns tend to reduce the accuracy of bow shock resolution, which leads to inaccurate computation of entropy across the shock wave and inaccurate flow simulations. Hence, grid line straightness in the body to shock direction as monitored by

$$\Theta = \frac{S\,\big|_{(\zeta_{min}\rightarrow\zeta_{max})}}{\sum_{\zeta=1}^{\zeta_{max}} |\vec{r}|_\zeta} \tag{3}$$

is the third measure used to determine if a volume grid is usable for hypersonic flow simulations.

Geometry for Method Assessment

For the discussion of the techniques used to control grid quality a generic 8^o half angle sphere-cone geometry is used, and shown in figure 1, with computational coordinates and flow domain shown in figure 2.

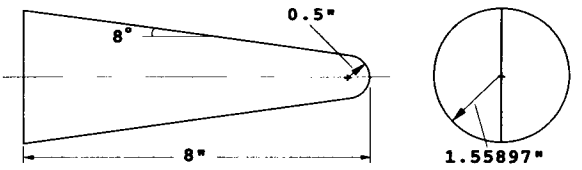

Fig. 1 Two view drawing of an 8^o sphere-cone used for grid generation discussions and assessment of solution strategies

Structured Volume Grid Smoothing Equations

Elliptic PDEs are derived from the superposition of Poisson equations, which produces inherently smooth variations of isothermal line intersections, or grid lines

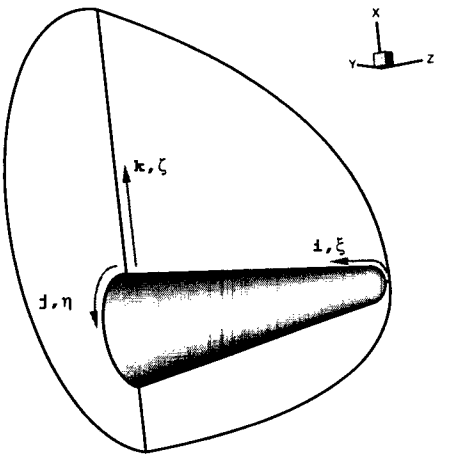

Fig. 2 Three-dimensional limits of the flow domain with physical and computational directions noted, for an angle of attack.

and grid points, and take the form of

$$\xi_{xx} + \xi_{yy} + \xi_{zz} = P \tag{4a}$$
$$\eta_{xx} + \eta_{yy} + \eta_{zz} = Q \tag{4b}$$
$$\zeta_{xx} + \zeta_{yy} + \zeta_{zz} = R \tag{4c}$$

Equation 4 is not solved easily because determining the derivatives of the computational domain (ξ,η,ζ), where points are evenly spaced, in terms of the physical coordinates (x,y,z), where points are non-uniformly spaced, is difficult. By using a coordinate transformation the following transformed Poisson System, written in vector form results:

$$\alpha_{11}\vec{r}_{\xi\xi} + \alpha_{22}\vec{r}_{\eta\eta} + \alpha_{33}\vec{r}_{\zeta\zeta} + 2\left(\alpha_{12}\vec{r}_{\xi\eta} + \alpha_{13}\vec{r}_{\xi\zeta} + \alpha_{23}\vec{r}_{\eta\zeta}\right) = -J^2(P\vec{r}_\xi + Q\vec{r}_\eta + R\vec{r}_\zeta) \tag{5}$$

where,

$$\vec{r} = [xyz]^T$$

and

$$\alpha_{11} = \gamma_{11}^2 + \gamma_{21}^2 + \gamma_{31}^2 \tag{6a}$$
$$\alpha_{22} = \gamma_{12}^2 + \gamma_{22}^2 + \gamma_{32}^2 \tag{6b}$$
$$\alpha_{33} = \gamma_{13}^2 + \gamma_{23}^2 + \gamma_{33}^2 \tag{6c}$$
$$\alpha_{12} = \gamma_{11}\gamma_{12} + \gamma_{21}\gamma_{22} + \gamma_{31}\gamma_{32} \tag{6d}$$
$$\alpha_{13} = \gamma_{11}\gamma_{13} + \gamma_{21}\gamma_{23} + \gamma_{31}\gamma_{33} \tag{6e}$$
$$\alpha_{23} = \gamma_{12}\gamma_{13} + \gamma_{22}\gamma_{23} + \gamma_{32}\gamma_{33} \tag{6f}$$
$$J = x_\xi\gamma_{11} + x_\eta\gamma_{12} + x_\zeta\gamma_{13} \tag{6g}$$

with,

$$\gamma_{11} = J\xi_x = y_\eta z_\zeta - y_\zeta z_\eta \quad (7a)$$
$$\gamma_{22} = J\eta_y = x_\xi z_\zeta - x_\zeta z_\xi \quad (7b)$$
$$\gamma_{33} = J\zeta_z = x_\xi y_\eta - x_\eta y_\xi \quad (7c)$$
$$\gamma_{12} = J\xi_y = y_\zeta z_\xi - y_\xi z_\zeta \quad (7d)$$
$$\gamma_{13} = J\xi_z = y_\xi z_\eta - y_\eta z_\xi \quad (7e)$$
$$\gamma_{21} = J\eta_x = x_\zeta z_\eta - x_\eta z_\zeta \quad (7f)$$
$$\gamma_{23} = J\eta_z = x_\eta z_\xi - x_\xi z_\eta \quad (7g)$$
$$\gamma_{31} = J\zeta_x = x_\eta y_\zeta - x_\zeta y_\eta \quad (7h)$$
$$\gamma_{32} = J\zeta_y = x_\zeta y_\xi - x_\xi y_\zeta \quad (7i)$$

The solution of these non-linear, non-homogeneous PDEs for the development of structured grids has been the focus of substantial and ongoing research. Some techniques are more viable than others, but each requires user specified conditions to determine a set of source terms for controlling the grid. Implicit source terms such as S&S and H&W are constructed by assuming Dirichlet boundary conditions, cell sizes and grid line incidence angles at a boundary. The resulting source terms are updated as the solution of the elliptic PDEs converges, based on the current state of the initial volume grid. Explicit source terms such as T&M are constructed by assuming orthogonal intersections of all grid lines which causes many terms in equation 5 to be assumed to be zero, thus significantly reducing the complexity of the equation. Explicit source terms are computed prior to solving the elliptic PDEs and are held constant because they already assume an orthogonal grid. By comparison to implicit source terms which are dependent on the boundary where they are formulated, explicit source terms are based on volumetric assumptions. Hence, the source term in use at any face can differ from another boundary, but explicit source terms of T&M use the same formulation throughout the computational domain.

Solution Strategy

Solving the system of elliptic PDEs for constructing structured volume grids can be done using a variety of textbook techniques, but each requires a linearization of equation 5. These equations are linearized by assuming the cofactors (α_{ij}), the source terms P, Q, and R, and the Jacobian of the transformation to be constants, computed based on the previous iteration. An initial solution to the grid points is required for this linearization, and is typically provided by Three-Dimensional Trans-Finite Interpolation[5] (3DTFI). The 3DTFI method for grid initialization uses bi-linear blending functions given by

$$\Phi_u = \begin{cases} 1-\bar{\xi} & u=0 \\ \bar{\xi} & u=1 \end{cases} \quad (8a)$$
$$\Phi_v = \begin{cases} 1-\bar{\eta} & v=0 \\ \bar{\eta} & v=1 \end{cases} \quad (8b)$$
$$\Phi_w = \begin{cases} 1-\bar{\zeta} & w=0 \\ \bar{\zeta} & w=1 \end{cases} \quad (8c)$$

and,

$$\bar{\xi} = \left(\frac{\xi - \xi_{min}}{\xi_{max} - \xi_{min}}\right) \quad (9a)$$
$$\bar{\eta} = \left(\frac{\eta - \eta_{min}}{\eta_{max} - \eta_{min}}\right) \quad (9b)$$
$$\bar{\zeta} = \left(\frac{\zeta - \zeta_{min}}{\zeta_{max} - \zeta_{min}}\right) \quad (9c)$$

which are used in the 3DTFI equation,

$$\begin{aligned} \vec{r}(\xi,\eta,\zeta) &= \sum_{u=0}^{1} \Phi_u \vec{r}(\xi_u,\eta,\zeta) + \sum_{v=0}^{1} \Phi_v \vec{r}(\xi,\eta_v,\zeta) \\ &+ \sum_{w=0}^{1} \Phi_w \vec{r}(\xi,\eta,\zeta_w) \\ &- \sum_{u=0}^{1}\sum_{v=0}^{1} \Phi_u\Phi_v \vec{r}(\xi_u,\eta_v,\zeta) \\ &- \sum_{v=0}^{1}\sum_{w=0}^{1} \Phi_v\Phi_w \vec{r}(\xi,\eta_v,\zeta_w) \\ &- \sum_{u=0}^{1}\sum_{w=0}^{1} \Phi_u\Phi_w \vec{r}(\xi_u,\eta,\zeta_w) \\ &+ \sum_{u=0}^{1}\sum_{v=0}^{1}\sum_{w=0}^{1} \Phi_u\Phi_v\Phi_w \vec{r}(\xi_u,\eta_v,\zeta_w) \end{aligned} \quad (10)$$

where,

$$\xi_0 \Rightarrow \bar{\xi} = 0$$
$$\xi_1 \Rightarrow \bar{\xi} = 1$$

The value of u, v, and w, identify the limits of the computational directions such that when any are zero, the corresponding computational direction indicated is the minimum boundary. Likewise, when u, v, or w are unity, the opposing, or maximum limit, boundary is identified.

Given an initial grid, the linearized PDEs are solved using a Point Implicit Successive Over Relaxation (PSOR) scheme. Judicious choice of the relaxation factor, ω, can enable solution acceleration via over relaxation. The ω can be a constant, or based on some local optimal value.[6] The optimal value to use is usually derived by considering the fact that the PSOR reduces the linearized version of equation 5 down to a set of ordinary differential equations (ODEs). Assuming

a constant coefficient Jacobi matrix for the ODEs only for estimating an optimal relaxation factor, the eigenvalues for the elliptic system of linearized equations can be determined. Then the local optimal relaxation factor is based on the largest eigenvalue which characterizes the slowest rate to convergence of the system at the local point. Use of a constant coefficient matrix to approximate the system of PDEs towards optimal relaxation implies that the grid can not have significant stretching, in order for the constant coefficient matrix assumption to be accurate. If a grid has uniform to moderately stretched grids, optimal relaxation can be used to accelerate solution convergence, an added advantage to minimizing stretching at all boundaries of the computational domain.

Traditional Techniques

Traditionally, the elliptic PDEs are solved by initializing a grid with 3DTFI, specifying boundary conditions, computing source terms at the boundary, propagating them onto the interior of the domain, then solving the elliptic PDEs for the specified conditions. The remaining issue in this process is which source terms to use and the blending of source terms onto the interior. As noted earlier, implicit source terms are computed at the boundary and decayed onto the interior, while explicit source terms are computed at the boundary and interpolated onto the interior such that P, Q, and R exist at all points on the interior. Source term hybridization is the coupling of the implicit which can accurately impose cell size and incidence angle constraints at a boundary and explicit source terms which can impose grid line intersection control on the interior. A bridging function is then used to decay the implicit source terms from the boundary onto the interior, while the explicit source terms are blended from complete control at the interior to no control at the boundaries.[7] This bridging is accomplished using

$$P_{i,j,k} = \sum_{l=1}^{6} \left(p^{\mathrm{I}} - p^{\mathrm{E}}\right)(l) + P^{\mathrm{E}}_{i,j,k} \tag{11}$$

where the implicit (Imp.) and explicit (Exp.) source terms are based on $p(l)$ with l identifying the face as given by

$$\left(p^{\mathrm{I}} - p^{\mathrm{E}}\right)(1) = \left(p^{\mathrm{I}}_{\xi_{\min}} - p^{\mathrm{E}}_{\xi_{\min}}\right) e^{-\beta_1(\xi-1)} \tag{12a}$$

$$\left(p^{\mathrm{I}} - p^{\mathrm{E}}\right)(2) = \left(p^{\mathrm{I}}_{\xi_{\max}} - p^{\mathrm{E}}_{\xi_{\max}}\right) e^{-\beta_2(\xi_{\max}-\xi)} \tag{12b}$$

$$\left(p^{\mathrm{I}} - p^{\mathrm{E}}\right)(3) = \left(p^{\mathrm{I}}_{\eta_{\min}} - p^{\mathrm{E}}_{\eta_{\min}}\right) e^{-\beta_3(\eta-1)} \tag{12c}$$

$$\left(p^{\mathrm{I}} - p^{\mathrm{E}}\right)(4) = \left(p^{\mathrm{I}}_{\eta_{\max}} - p^{\mathrm{E}}_{\eta_{\max}}\right) e^{-\beta_4(\eta_{\max}-\eta)} \tag{12d}$$

$$\left(p^{\mathrm{I}} - p^{\mathrm{E}}\right)(5) = \left(p^{\mathrm{I}}_{\zeta_{\min}} - p^{\mathrm{E}}_{\zeta_{\min}}\right) e^{-\beta_5(\zeta-1)} \tag{12e}$$

$$\left(p^{\mathrm{I}} - p^{\mathrm{E}}\right)(6) = \left(p^{\mathrm{I}}_{\zeta_{\max}} - p^{\mathrm{E}}_{\zeta_{\max}}\right) e^{-\beta_6(\zeta_{\max}-\zeta)} \tag{12f}$$

and the volumetric explicit source term is formed by the same 3DTFI method used for grid initialization

$$\begin{aligned} P^{\mathrm{E}}_{i,j,k} &= \sum_{u=0}^{1} \Phi_u p^{\mathrm{E}}(\xi_u, \eta, \zeta) + \sum_{v=0}^{1} \Phi_v p^{\mathrm{E}}(\xi, \eta_v, \zeta) \\ &+ \sum_{w=0}^{1} \Phi_w p^{\mathrm{E}}(\xi, \eta, \zeta_w) \\ &- \sum_{u=0}^{1}\sum_{v=0}^{1} \Phi_u \Phi_v p^{\mathrm{E}}(\xi_u, \eta_v, \zeta) \\ &- \sum_{v=0}^{1}\sum_{w=0}^{1} \Phi_v \Phi_w p^{\mathrm{E}}(\xi, \eta_v, \zeta_w) \\ &- \sum_{u=0}^{1}\sum_{w=0}^{1} \Phi_u \Phi_w p^{\mathrm{E}}(\xi_u, \eta, \zeta_w) \\ &+ \sum_{u=0}^{1}\sum_{v=0}^{1}\sum_{w=0}^{1} \Phi_u \Phi_v \Phi_w p^{\mathrm{E}}(\xi_u, \eta_v, \zeta_w) \end{aligned} \tag{13}$$

In source term hybridization the explicit source terms are always additive and dominant on the interior. At the boundary the implicit source terms are dominant. This blending scheme is one of the methods that exists in the 3DGRAPE/AL[8] software, which is used to generate all the structured grids in this paper. To maintain consistency for the analysis of the generated grids, and the solver performance, the source term decay rate β_l is identical for each face, a typical choice in practice. All computations are performed on a 270Mhz Silicon Graphics R12K machine with 32-bit precision.

Using equation 11 to blend the source terms, volume grids were generated for the domain identified in figure 2 by varying grid point movement relaxation from 0.8 to 1.4 and source term decay rates from 0.05 to 0.45. The grid point movement relaxation rates were chosen to span the effects of the PSOR from under relaxed to over relaxed. The source term decay rates were chosen to represent typical default values of 0.45 used by many elliptic PDE solvers, down to 0.05 as the practical limit using source term hybridization for obtaining a converged solution to the elliptic PDEs. Utilizing S&S source terms to impose orthogonal grid line incidence at all boundaries except the $\zeta_{\max}$ and pole faces, the performance of the solver is tracked with the number of iterations to a converged state. Convergence of the point movement was chosen based on the precision accuracy of the root mean square of the update to all movement in the domain. For the SGI at 32-bit precision and the size of the geometry, this value is $1x10^{-6}$. Convergence of the source terms was selected to be 3 orders of magnitude difference between the largest source term and the root-mean square of the updates to the source terms.[9] Initially,

4 orders of magnitude difference was chosen to identify source term convergence, but the PDE solver could not obtain this level of convergence in the source terms when using source term hybridization. Both grid point movement and source term convergence are used because it is possible to advance the solution such that the point movement appears to be converged, but the source term corrections are still large. Setting $\omega \ll 1$ may falsely imply grid points are not moving, but source term updates convergence is not yet obtained.

The convergence criteria established above, resulted in the grid point movement and source term convergence performance shown in figures 3 and 4 for grid point movement and source term convergence, respectively. The time required for each iteration with

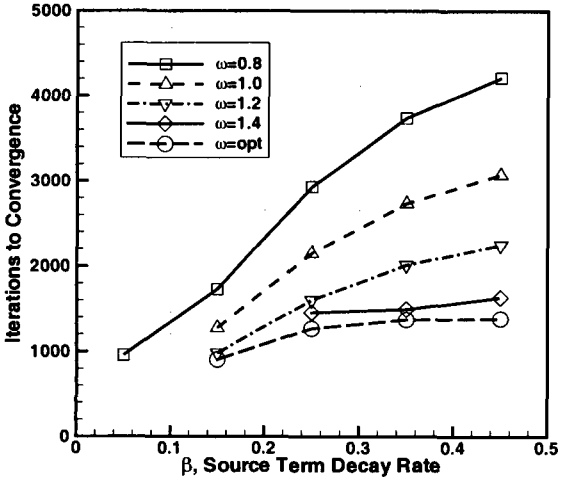

Fig. 3 Grid point movement convergence for source term hybridization.

source term hybridization is 2.37 seconds. As anticipated, increasing the relaxation rate for grid point movement results in accelerated solution convergence. With the optimum relaxation factor, the least number of iterations to convergence is fairly consistent for most of the source term decay rates. Second, the implicit source terms tend to converge faster than the grid point movement, due to the smaller region required for convergence. Implicit source terms only need to be resolved near the boundary due to the decay rates, whereas the grid point movement needs to converge over the entire volume.

Contrary to intuition, decreasing the decay rate of the source terms, thereby increasing the influence of the source terms, increases the rate of convergence[10] of the grid point movement. It has long been assumed in the field of grid generation that decreasing the rate of decay of the source terms can cause solver divergence. Yet for the simple sphere-cone geometry shown here, the opposite occurs. This effect lays in the application of the source terms. Basically, increasing the influence of the source terms increases the movement of more of the grid earlier in the iteration cycles. Hence, convergence is obtained at an increased rate.

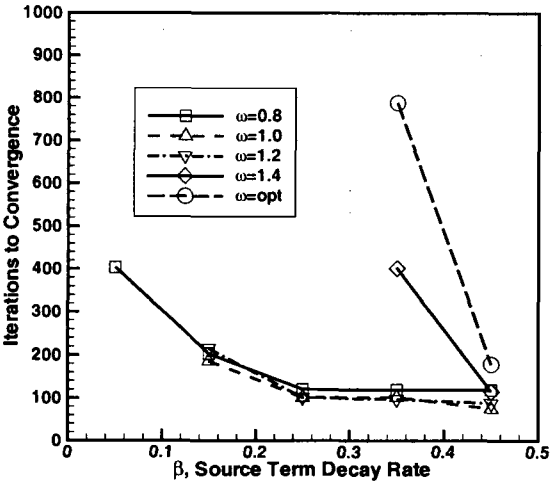

Fig. 4 Source term convergence for source term hybridization.

Most notable in these figures it the fact that the strongest influence source terms do not produce a solution for relaxation rates above 0.8 which indicates a significant deficiency; significant increases in grid point movement iterations are needed to obtain convergence. Strong influence of the source terms at the boundaries causes the explicit source terms to be overcome by the implicit source terms. The basic problem that has arisen is that explicit source terms are assuming orthogonality, while the source terms at the boundary are not necessarily set to orthogonality. As a result, there are significant conflicts between the source terms that have to be resolved by the PDE solver. Evident by the increase in the number of iterations to convergence of the grid, is the work required to resolve the conflicts, where implicit source terms have a weak influence. Hence, with the trends established for increasing source term influence and relaxation rates, there is a limit of efficiency when using source term hybridization because lower relaxation rates require significant increases in iterations of the grid movement to convergence. This implies that in order to obtain convergence the user may use too small ω to ensure convergence.

Source term hybridization was designed to improve grid quality control throughout the computational domain. As such, representative structured volume grids are shown in figures 5 and 6.

Based on visual inspection for β ranging from 0.15 to 0.45, representative i- and j-planes in the interior of the domain for a grid point movement relaxation

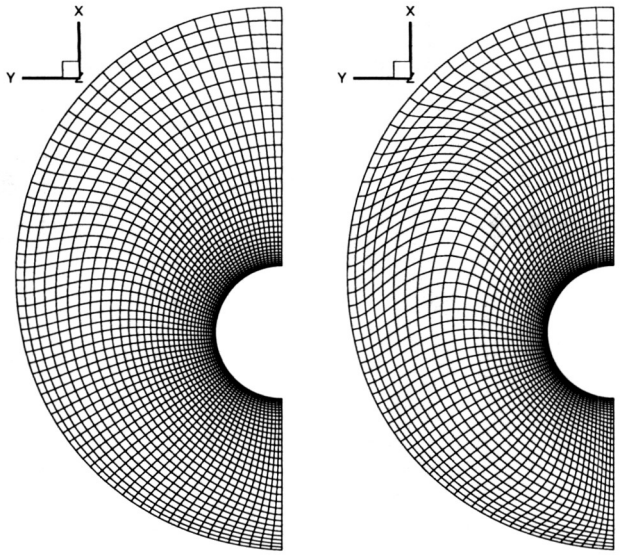

a) $\beta = .15$ **b)** $\beta = .45$

Fig. 5 Planes at $i = 65$ for $\omega = 1.0$ for source term hybridization.

rate of 1.0, the grid lines in the body-to-shock direction are curved, the stretching is varying, and most importantly, the grids are not close to orthogonality on the interior of the domain. Again, this is due to the explicit source terms conflicting with the implicit source terms, which is evident by the weaker influence implicit source terms where $\beta = .45$; the typical default value for implicit source term decay. For the stronger influence implicit source terms, the orthogonality is improved and curvature is reduced, but there still remains some skewness that could adversely affect body-to-shock direction grid adaptation, and the accuracy of a predicted flow field.

These results also indicate a serious problem is emerging; the robustness of the scheme is diminished because the strong influence source terms are not converging for the grid point movement relaxation factor of 1.0 or higher. Fully converged solutions are not possible at all the conditions specified, which indicates that the limit to using source term hybridization is easily reached for this simple sphere-cone shape. Thus there are considerable drawbacks to source term hybridization.

A New Technique

Generating structured volume grids of high fidelity has been time consuming and difficult because of the techniques available for grid control. Although it may seem advantageous to attempt the negating of undesired characteristics, a scheme would have to be robust enough to handle different boundary types, orientations, and quite possibly boundary topography.

Alternatively, a scheme could be developed that would have the desired effects of angle control while maintaining cell size at the boundaries of the computational domain, and reducing the time required to

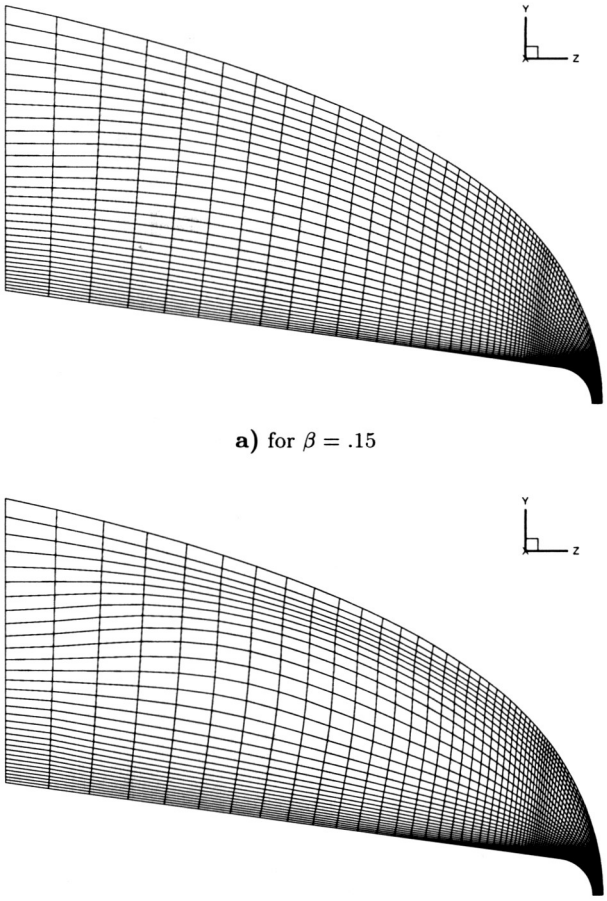

a) for $\beta = .15$

b) $\beta = .45$

Fig. 6 Planes at $j = 65$ for $\omega = 1.0$ for source term hybridization.

obtain a converged solution of the elliptic PDEs. In both the hybridization and any alternative method, angle control is imperative, but boundaries require an additional control for the cell size. This leads to the realization that decoupling the angle controls from the cell size controls may prove to be a worthwhile avenue of research to pursue. There are many mechanisms to decouple the source term controls, but in most cases the source terms have to work together towards the development of a grid. A approach for multiple variable, multiple function blending of data is Trans-Finite Interpolation. Hence, a form of TFI is selected to do the blending of the implicit source terms at all faces such that cell sizes influence only the boundaries, and angle control influences all regions. This approach produces an anisotropic set of blending functions ($\Psi_{u,v,w}$ and $\Omega_{u,v,w}$) for equation 13. The simplest method to accomplish the decoupling and achieve the anisotropy is to substitute the $\Phi_{u,v,w}$ terms of equation 13 to the required source terms and use decayed interpolation

using linear Lagrange basis functions, yielding

$$\Psi_u = \begin{cases} (1-\bar{\xi})e^{-\beta_1(\xi-1)} & u=0 \\ \bar{\xi}e^{-\beta_2(\xi_{max}-\xi)} & u=1 \end{cases} \quad (14a)$$

$$\Psi_v = \begin{cases} (1-\bar{\eta})e^{-\beta_3(\eta-1)} & v=0 \\ \bar{\eta}e^{-\beta_4(\eta_{max}-\eta)} & v=1 \end{cases} \quad (14b)$$

$$\Psi_w = \begin{cases} (1-\bar{\zeta})e^{-\beta_5(\zeta-1)} & w=0 \\ \bar{\zeta}e^{-\beta_6(\zeta_{max}-\zeta)} & w=1 \end{cases} \quad (14c)$$

and quadratic Lagrange interpolation for the cell sizes with an exponential decay function, as given by

$$\Omega_u = \begin{cases} 2\left(\bar{\xi}-\frac{1}{2}\right)\left(\bar{\xi}-1\right)e^{-\beta_1(\xi-1)} & u=0 \\ 4\bar{\xi}\left(1-\bar{\xi}\right) & u=1 \\ 2\bar{\xi}\left(\bar{\xi}-\frac{1}{2}\right)e^{-\beta_2(\xi_{max}-\xi)} & u=2 \end{cases} \quad (15a)$$

$$\Omega_v = \begin{cases} 2\left(\bar{\eta}-\frac{1}{2}\right)\left(\bar{\eta}-1\right)e^{-\beta_3(\eta-1)} & v=0 \\ 4\bar{\eta}\left(1-\bar{\eta}\right) & v=1 \\ 2\bar{\eta}\left(\bar{\eta}-\frac{1}{2}\right)e^{-\beta_4(\eta_{max}-\eta)} & v=2 \end{cases} \quad (15b)$$

$$\Omega_u = \begin{cases} 2\left(\bar{\zeta}-\frac{1}{2}\right)\left(\bar{\zeta}-1\right)e^{-\beta_5(\zeta-1)} & w=0 \\ 4\bar{\zeta}\left(1-\bar{\zeta}\right) & w=1 \\ 2\bar{\zeta}\left(\bar{\zeta}-\frac{1}{2}\right)e^{-\beta_6(\zeta_{max}-\zeta)} & w=2 \end{cases} \quad (15c)$$

where,

$\xi_0 \Rightarrow \bar{\xi}=0$
$\xi_1 \Rightarrow \bar{\xi}=\frac{1}{2}$
$\xi_2 \Rightarrow \bar{\xi}=1$

In a Lagrange polynomial, linear interpolation requires two source terms, the beginning and ending values. However, quadratic blending requires three source terms, where the first and last are identical to the bi-linear and the middle is set to zero. Hence, the blending of the source term that controls cell size decays to zero on the interior (i.e., no control), from both ends of a specified direction, and no decay function is needed. Using equation 13 and applying the ALBTFI technique, the equation in use for the source terms controlling the ξ direction is given by equation 16, as a stencil for the other source terms in the η- and ζ-directions.

$$\begin{aligned} P_{i,j,k} &= \sum_{u=0}^{2}\Omega_u p^{\mathrm{I}}(\xi_u,\eta,\zeta) + \sum_{v=0}^{1}\Psi_v p^{\mathrm{I}}(\xi,\eta_v,\zeta) \\ &+ \sum_{w=0}^{1}\Psi_w p^{\mathrm{I}}(\xi,\eta,\zeta_w) \\ &- \sum_{u=0}^{2}\sum_{v=0}^{1}\Omega_u\Psi_v p^{\mathrm{I}}(\xi_u,\eta_v,\zeta) \\ &- \sum_{v=0}^{1}\sum_{w=0}^{1}\Psi_v\Psi_w p^{\mathrm{I}}(\xi,\eta_v,\zeta_w) \\ &- \sum_{u=0}^{2}\sum_{w=0}^{1}\Omega_u\Psi_w p^{\mathrm{I}}(\xi_u,\eta,\zeta_w) \\ &+ \sum_{u=0}^{2}\sum_{v=0}^{1}\sum_{w=0}^{1}\Omega_u\Psi_v\Psi_w p^{\mathrm{I}}(\xi_u,\eta_v,\zeta_w) \end{aligned} \quad (16)$$

In equation 16, the Ω terms control the cell size and decays rapidly with the combination of a quadratic interpolation coupled with an exponential decay function, and the Ψ terms control angles which decay at a slower rate.

The anisotropic approach was used in two dimensions in prior work[3] with only H&W source terms with an elliptic PDE system that factored the Jacobian of the transformation out of the equation, and no decay functions. This prior work made use of a strongly implicit procedure (SIP) to obtain a convergent solution to the elliptic PDEs. An SOR method in prior work was unable to produce a converged solution because of the stiffness created by the H&W source terms. Choice of SIP or SOR solution methods should not produce different grids, but will affect convergence. Instead of switching to the SIP solution technique in the present work, the PSOR method is retained for consistency with previous computations, because S&S source terms are being retained for orthogonal grid line control. Recall that the S&S source terms are being applied at all faces except the pole boundary where no source term is used and the outer boundary where H&W source terms are used to impose non-orthogonal grid line incidence control. The current work incorporates the decay function to improve convergence using the PSOR by reducing the intensity of the H&W source terms; the source terms that proved difficult to use in prior work with SOR methods. The decoupling in the ALBTFI technique is tempered with the inclusion of a decay function in equations 14 and 15, a mechanism that aids convergence without the use of an SIP. Utilizing ALBTFI to generate the sphere-cone volume grid, with the same set of grid point relaxation rates and source term influence as was used for the source term hybridization, the solver performance for grid point movement and source term convergence are shown in figures 7 and 8, respectively.

The ALBTFI technique requires 0.33 seconds/iteration (14%) more than source term hybridization because the complexity of the blending function has increased significantly. By comparison to the hybridization strategy, several performance issues can be addressed. First, the number of iterations and the time required to obtain convergence of the elliptic PDEs is shown in table 1. For the strong influence of the source terms, where the best grid is usually produced, the time to convergence for the ALBTFI scheme is faster than the hybrid approach, because the hybrid approach did not produce a converged solution for the relaxation rate of unity. Source term convergence is much smoother for the ALBTFI method, faster in most cases, and the ALBTFI method is significantly more robust than the hybrid approach which is evident by the obtained convergence. During the implementation of the ALBTFI

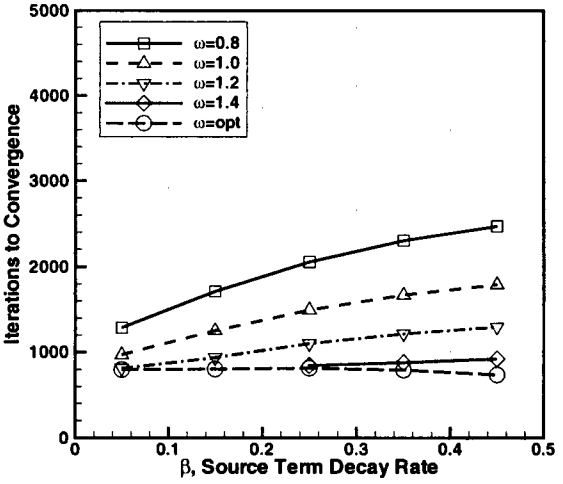

Fig. 7 Grid point movement convergence for ALBTFI.

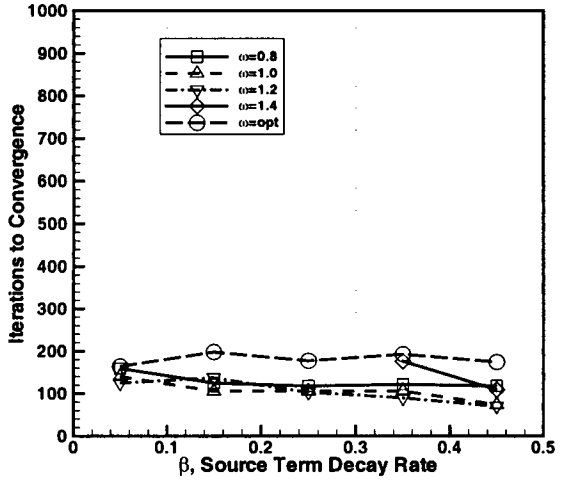

Fig. 8 Source term convergence for ALBTFI.

method, a Jacobi iterative technique was attempted, but failed to converge for relaxation rates above 1.0, which is attributed to the stiffness of the scheme. Stiffness is suspect because the two dimensional solver used in prior work required an SIP to get a converged solution. When a Gauss-Seidel iterative technique was implemented in the current work, the results shown in this paper were obtained. Although the blending function has become much more complex, there is no need to constantly difference the implicit and explicit source terms at a boundary, no need to compute T&M source terms, thereby significantly reducing the computer memory required. The performance of the elliptic PDE solver for the ALBTFI technique clearly indicates an improved convergence rate and significant robustness improvement. Comparing

Table 1 Convergence performance measures for 3DGRAPE/AL at a grid point movement relaxation of $w = 1.0$ for hybridization and ALBTFI source term blending schemes.

Blending Scheme	Number of Iterations	CPU Time (seconds)	Factor Decrease Over Hybrid
Hybrid	—	—	—
ALBTFI	968	2613.60	—

(a) Strong influence of source terms ($\beta = 0.05$).

Blending Scheme	Number of Iterations	CPU Time (seconds)	Factor Decrease Over Hybrid
Hybrid	2149	5093.13	1.0
ALBTFI	1495	4036.50	0.21

(b) Moderate influence of source terms ($\beta = 0.25$).

Blending Scheme	Number of Iterations	CPU Time (seconds)	Factor Decrease Over Hybrid
Hybrid	3075	7287.75	1.0
ALBTFI	1791	4835.70	0.34

(c) Weak influence of source terms ($\beta = 0.45$).

the performance of source term hybridization and the ALBTFI technique illustrated in figure 9, the ALBTFI scheme is generally more efficient, but particularly more robust for $\beta < 0.15$. The Hybrid scheme shows comparable efficiency to the ALBTFI at $\beta = 0.15$, however, the hybrid scheme source terms do not converge for decay rates that result in the highest quality grids. Hence, the hybrid scheme is not as robust as the ALBTFI method. Also note that in order to do these comparisons, the source term convergence criteria had to be reduced by one order of magnitude. Sacrificing the extent to which a solution is converged typifies the reduced robustness of the source term hybridization. Representative planes from the structured volume grids produced with ALBTFI are shown in figures 10 and 11 for the resulting i- and j-plane grids, respectively.

Evaluating the quality of the grids generated is difficult because no single measure identifies the trades needed in grid line intersection, stretching, and body-to-shock direction grid adaptation. However, by using these types of measures, and considering the minimum average orthogonality and the maximum average stretching which are both planar dependent, and the minimum average straightness, a global measure can be constructed, as given by

$$GQ = \frac{\bar{\theta}_{\min}\bar{\Theta}}{\bar{\epsilon}_{\max}} \tag{17}$$

Using this measure to quantify what can be visually in-

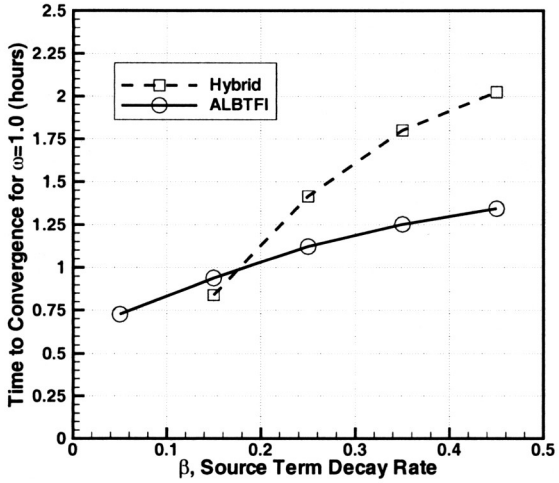

Fig. 9 Elliptic PDE solver performance measured in time to convergence for $\omega = 1.0$, grid point movement relaxation.

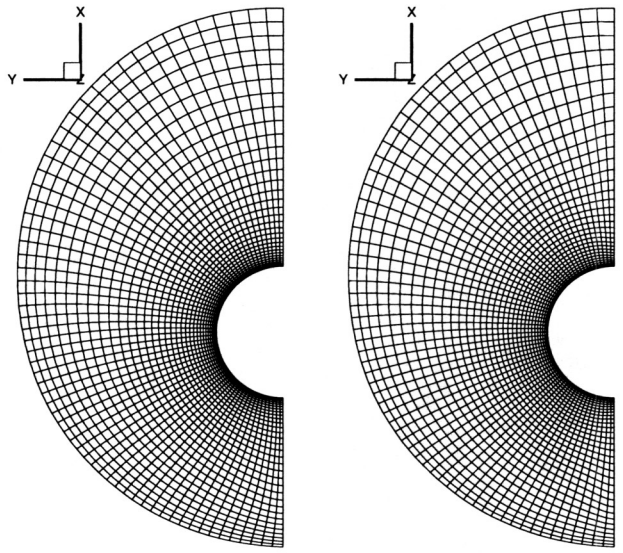

a) $\beta = .15$ **b)** $\beta = .45$

Fig. 10 Planes at $i = 65$ for $\omega = 1.0$ for ALBTFI.

spected, figure 12 illustrates the grid quality measure,

Inspection of the grids provides conclusive proof that the grid quality from the ALBTFI approach is indeed as good if not better than the source term hybridization, and also illustrates that even weak influence of the implicit source terms can produce viable structured grids using ALBTFI. The ALBTFI method is more robust than the source term hybridization, based on the time required to obtain converged solutions, the extent of convergence of the source terms as noted by the sacrifice of the order of magnitude of source term corrections in order to do any comparison, and the quality of the volume grids produced. Therefore, ALBTFI can generate high fidelity grids more efficiently than the standard source term hybridization.

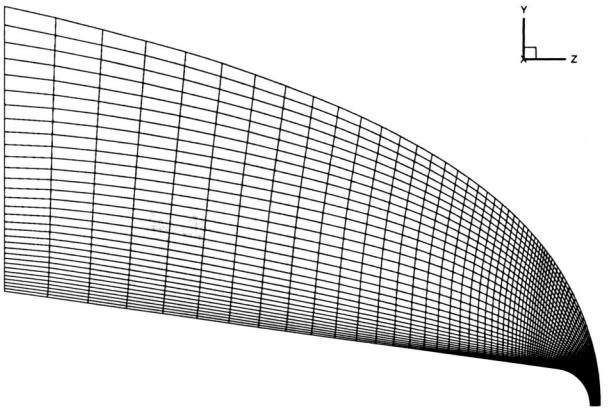

a) $\beta = .15$

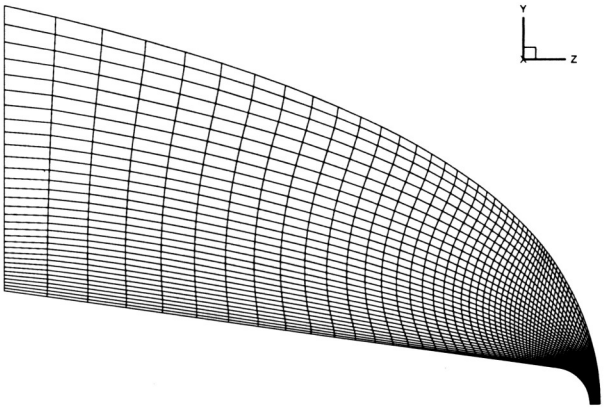

b) $\beta = .45$

Fig. 11 Planes at $j = 65$ for $\omega = 1.0$ for ALBTFI.

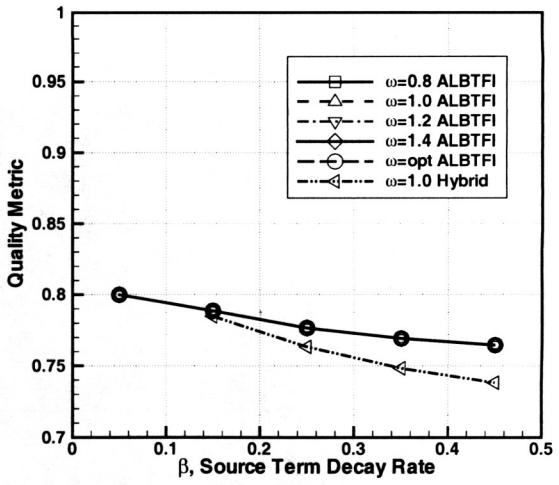

Fig. 12 Volume grid quality analysis using source term hybridization.

Application to a Complex Shape

Robustness and efficiency in the generation of high fidelity structured volume grids are improved by the ALBTFI scheme. To further test the robustness as compared with source term hybridization, a more complex geometry (Space Shuttle Orbiter) is examined with both source term controls. This volume grid has grid dimensions that are eight times larger than the sphere-cone used to evaluation of the ALBTFI technique, tighter spacings at the wall to simulate the generation of a viscous grid, and larger variations in grid stretching throughout the domain; significant complicating issues for grid generation. The same grid point movement relaxation factors and source term decay rates were used for grid construction, yet not all cases converged and grids were not produced, due to the complexity of the volume grid to be generated. Boundary orthogonality was imposed on the faces that represent the wall, symmetry planes, and exit of the flow domain, while non-orthogonal angles were imposed at the outer boundary to reduce grid line curvature. Utilizing the same source term decay rates from all faces, and these boundary conditions, volume grids were generated. The most noticeable result from this grid generation was that the hybridization technique never converged for either grid point movement or source terms, and a usable grid was not produced. The lack of convergence can be attributed to the original formulation of the T&M source terms which were designed for internal flows with simple cross-sectional shapes, as well as the conflicts between grid controls at the boundaries. However, the ALBTFI method did converge, and the performance of the volume grid generator is illustrated in figures 13 and 14 for the grid point movement and source term convergence, respectively.

Based on the performance of the ALBTFI technique within the 3DGRAPE/AL software, the time required to generate the grids is approximately 20.22 seconds per iteration, or 45 hours for fastest case, and 98 hours for the slowest. The fact that the ALBTFI technique converges, and illustrates the same trend for the family of curves of grid point movement relaxation where convergence is accelerated with increasing relaxation factor changes, is evidence of the robustness of this technique. However, based on the source term decay rate, the fastest convergence occurs for $\beta = 0.35$. This may be attributed to the complexity of the volume grid boundaries and controls required to obtain a volume grid. Even though source term decay rates stronger than 0.25 did not meet convergence criteria, usable volume grids were produced.

Visual inspection of the volume grids is not simple because of the density of the volume grid. Dimensions in the I- and J-direction were reduced by a factor of 4 to improve the clarity of the visual inspections. Three dimensional surfaces for the I- and J-planes were extracted according to the locations shown in figure 15. According to figure 16 for the I-plane and 17 for the J-plane, the stronger influence source terms produce straighter grid lines in the body to outer boundary direction, and tend to produce a longer propagation of orthogonality onto the interior. The I-plane illustrated, is located just aft of the fuselage/wing intersection, and shows that even though the grid is stretched in the cross-section, the stretching can be propagated, onto the interior which improves the quality of the grid for grid adaptation purposes. Additionally, the J-plane, which occurs along the water line of the vehicle, including the wing leading edge, illustrates that the grid maintains orthogonality through boundary layer region. These artifacts of the grid clearly indicate that

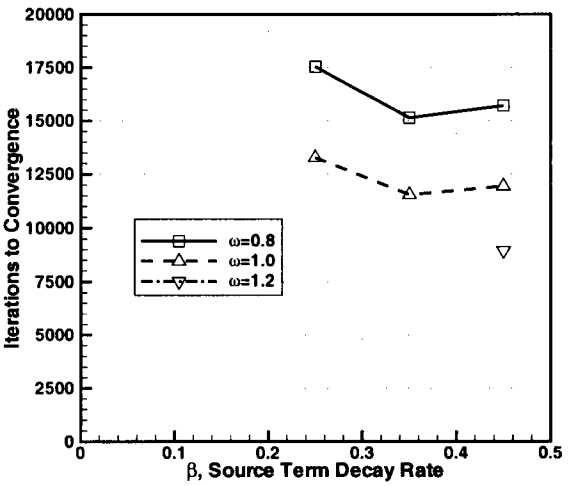

Fig. 13 Grid point movement convergence for ALBTFI on a Space Shuttle Orbiter.

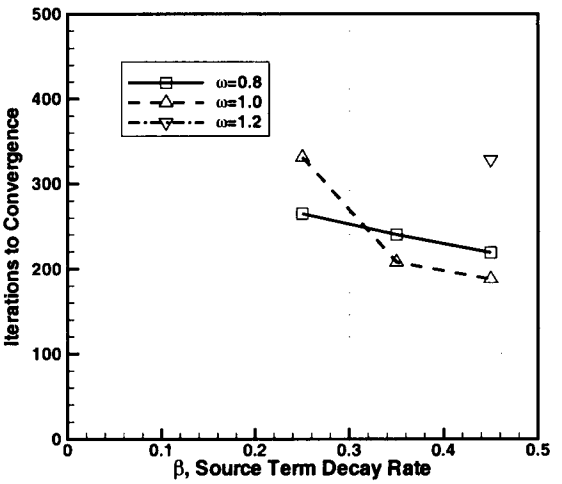

Fig. 14 Source term convergence for ALBTFI on a Space Shuttle Orbiter.

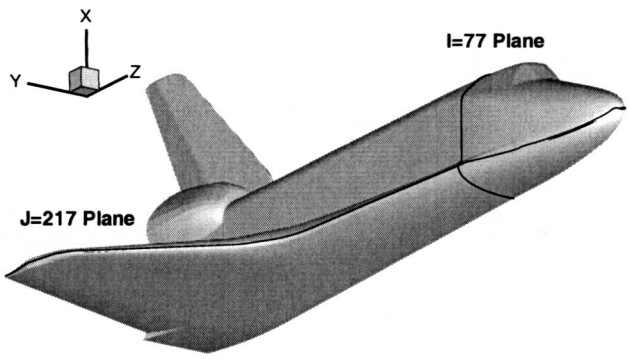

Fig. 15 Locations where I- and J-planes were extracted for visualizing the grids produced.

a high fidelity grid can be produced for such a complex shape as the space shuttle orbiter.

Conclusions

The Anisotropic Lagrange Based Trans-Finite Interpolation (ALBTFI) scheme is fully extended to three dimension to efficiently generate high fidelity grids with sufficient point density to resolve hypersonic flow field phenomenon. The technique is an alternate to source term hybridization, designed to control grid line intersections on the interior of a volume grid while maintaining an additional cell size constraint at the boundary. The ALBTFI scheme does not suffer from the problems encountered by source term hybridization such as source term conflicts and robustness, because only the desired characteristics of the controlling source terms are used, whereas the source term hybridization combines both the desired features such as boundary and interior domain grid line control with undesirable features such as inconsistent grid line incidence specification of separately formulated source terms.

The ALBTFI method offers numerous advantages over the typical source term hybridization by decoupling the cell size controlling source terms at opposing boundaries, and utilizing the entire domain for the blending, as opposed to blending boundary source terms to interior based source terms. The anisotropic nature of the ALBTFI method is derived from utilizing bi-quadratic blending for the control of cell sizes and bi-linear control for angles. Bi-quadratic blending of the cell sizes decouples the cell size specification between two opposing boundaries in the computational domain. Bi-linear blending of the angles maintains the straightest intersections between opposing boundaries, much like the effects that Thomas and Middlecoff (T&M) controls have. Since only the implicit source terms of Steger and Sorenson (S&S) and Hilgenstock and White (H&W) are being used at the boundary of the flow domain, and no other interior source terms are used, the conflicts are eliminated, the time to convergence of the elliptic PDE solver is improved, and the quality of the grid is improved. The interior control that was marginally provided by the T&M hybridization is replaced with the bi-linear interpolation of the angle controls in the ALBTFI approach. The results presented have shown the ALBTFI to provide better grid quality in less time, evident by both a 50% reduction in the iterations required to obtain a converged solution by comparison to the hybrid approach, and the ability to obtain a converged solution on a complex vehicle. The success of the ALBTFI scheme is attributed to the interaction between the system of implicit source terms, the incorporation of exponential decay functions, and the Trans-Finite Interpolation

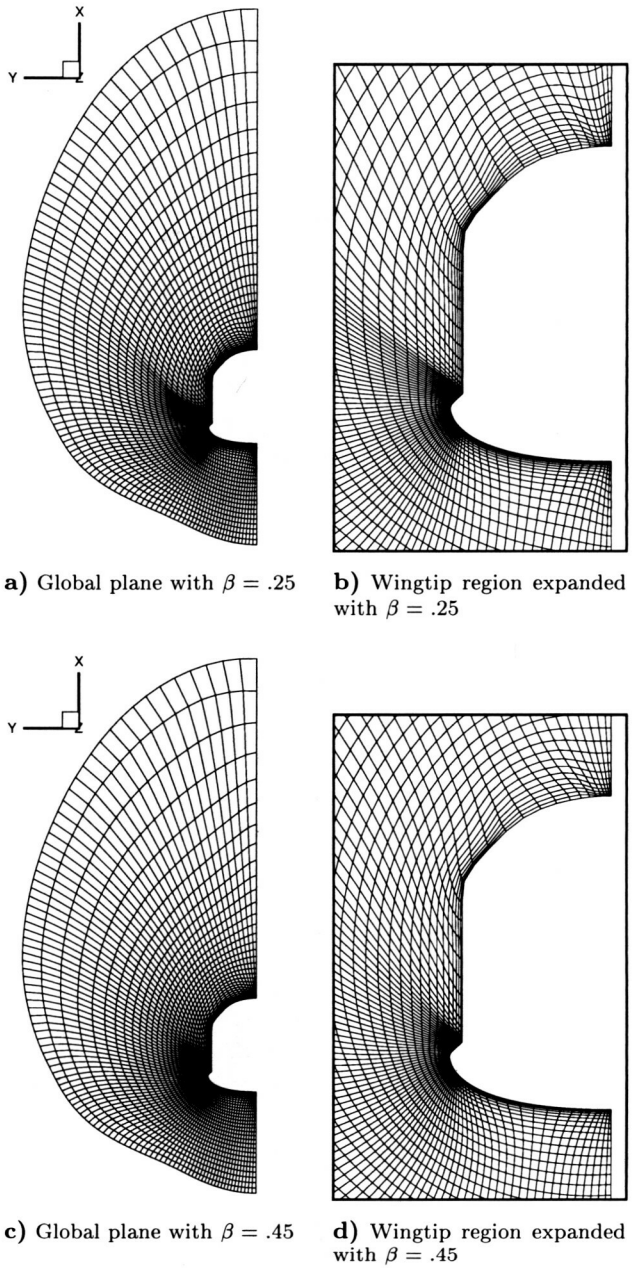

a) Global plane with $\beta = .25$

b) Wingtip region expanded with $\beta = .25$

c) Global plane with $\beta = .45$

d) Wingtip region expanded with $\beta = .45$

Fig. 16 Planes at $i = 77$ for $\omega = 1.0$ for ALBTFI reduced by 4 in J-direction.

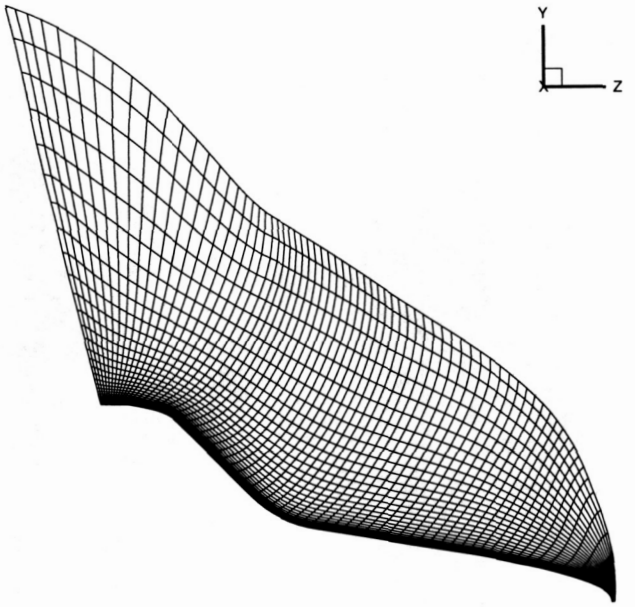

a) Global plane with $\beta = .25$

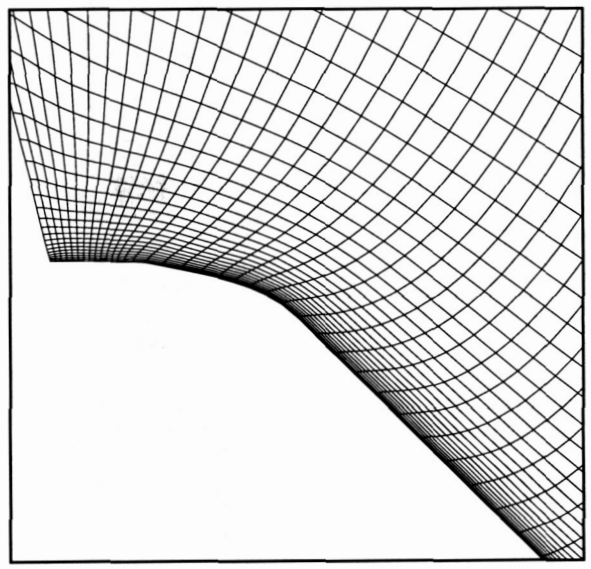

b) Wingtip region expanded with $\beta = .25$

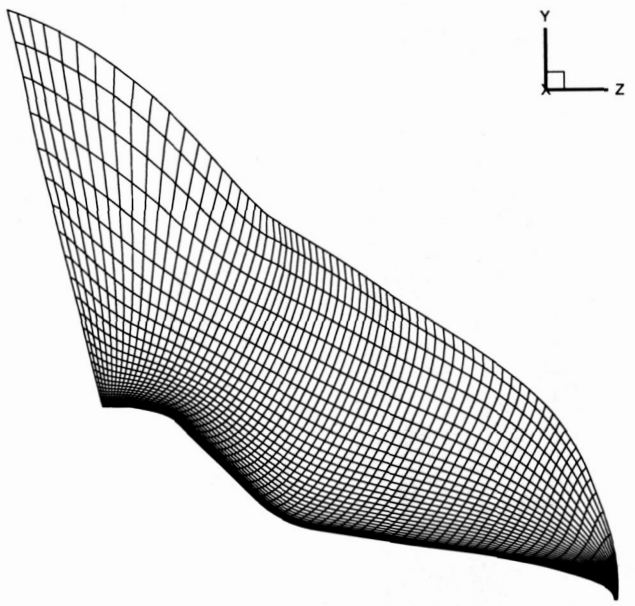

c) Global plane with $\beta = .45$

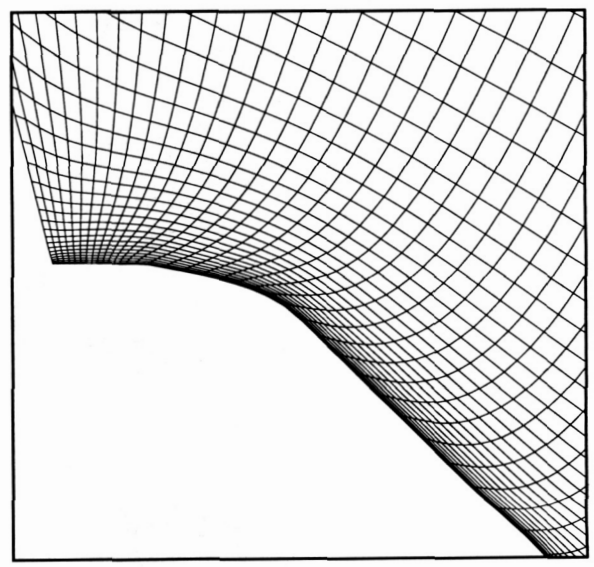

d) Wingtip region expanded with $\beta = .45$

Fig. 17 Planes at $j = 297$ for $\omega = 1.0$ for ALBTFI reduced by 4 in I-direction.

blending scheme. By tailoring the interpolation functions to the types of source terms in use, coupled with the advantages of the implicit source terms, the best blending scheme results.

Acknowledgment

This work was initially done for the partial completion of a Master of Science from the George Washington University (GWU). The author wishes to express his appreciation to John Whitesides, Ph.D. and Michael Myers, Ph.D., of GWU, James Thomas, Ph.D., K. James Weilmuenster, and the extensive support of the Aerothermodynamics Branch of the Aerodynamics, Aerothermodynamics, and Acoustics Competency at NASA Langley Research Center.

References

[1]Steger, J. L. and Sorenson, R. L., "Automatic Mesh-Point Clustering Near A Boundary in Grid Generation with Elliptic Partial Differential Equations," *Journal of Computational Physics*, Vol. 33, Academic Press, Inc., December 1979, pp. 405–410.

[2]Hilgenstock, A., "A Fast Method for the Elliptic Generation of Three-Dimensional Grids with Full Boundary Control," *Numerical Grid Generation in Computational Fluid Mechanics '88*, Pineridge Press Limited, 1988, pp. 137–146.

[3]White, J. A., "Elliptic Grid Generation with Orthogonality

and Spacing Control on an Arbitrary Number of Boundaries," AIAA Paper 90-1568, June 1990.

[4]Thomas, P. D. and Middlecoff, J. F., "Direct Control of the Grid Point Distribution in Meshes Generated by Elliptic Equations," *AIAA Journal*, Vol. 18, No. 6, June 1979, pp. 652–656.

[5]Soni, B. K., "Two– and Three–Dimensional Grid Generation for Internal Flow Applications of Computational Fluid Dynamics," AIAA Paper 85–1526, 1985.

[6]Ehrlich, L. W., "An Ad Hoc SOR Method," *Journal of Computational Physics*, Vol. 44, Academic Press, Inc., Nov.–Dec. 1981, pp. 31–45.

[7]J. P. Steinbrenner, Chawner, J. R., and Fouts, C. L., *The GRIDGEN 3D Multiple Block Grid Generation System*, chap. 5, No. WRDC–TR–90–3022, Wright Research and Development Center Report, July 1990, pp. 25–26.

[8]Sorenson, R. L. and Alter, S. J., "3DGRAPE/AL: The Ames/Langley Technology Upgrade," *Surface Modeling, Grid Generation, and Related Issues in Computational Fluid Dynamic (CFD) Solutions*, edited by Y. K. Choo, No. CP–3291, NASA, May 1995, pp. 447–462.

[9]Sorenson, R. L., "The 3DGRAPE Book: Theory, Users' Manual, Examples," NASA Technical Memorandum 102224, July 1989.

[10]Alter, S. J. and Weilmuenster, K. J., "Single Block Three–Dimensional Volume Grids About Complex Aerodynamic Vehicles," NASA Technical Memorandum 108986, May 1993.